Published in the Proceedings of the 16th International Aluminum Alloys Conference (ICAA16) 2018
ISBN: 978-1-926872-41-4
by the Canadian Institute of Mining, Metallurgy & Petroleum

EFFECTS OF Mg, Si, AND Cu ON THE FORMATION OF THE Al_3Sc/Al_3Zr DISPERSOIDS

*T. Dorin[1], M. Ramajayam[1], and T. J. Langan[2]

[1]Deakin University, Institute for Frontier Materials
Geelong, Victoria, 3216, Australia
*(*Corresponding author: thomas.dorin@deakin.edu.au)*

[2]Clean TeQ Ltd.
Australia

ABSTRACT

6xxx-series Al alloys are the most commonly used alloys in the automotive industry as they have an appropriate balance of strength, corrosion resistance and formability. The main strengthening phase in these alloys is the β'-Mg_2Si precipitates. One opportunity to achieve stronger 6xxx-series Al alloys, without affecting corrosion and formability, is the use of Sc. The main challenge of using Sc in 6xxx-series lies in the heat treatment, which must be designed to allow for a fine precipitation of both Al_3Sc and β'-Mg_2Si. In this work, two model alloys are used, an Al-Sc-Zr and an Al-Mg-Si-Cu-Sc-Zr, to explore the impact of the 6xxx-series key elements (Mg, Si and Cu) on the Al_3Sc precipitates. Transmission electron microscopy and atom probe tomography are used to investigate the precipitates present in the microstructure after casting. We find that higher Si content results in the formation of dispersoids upon casting. The average composition of these dispersoids is $(Al_{0.8},Si_{0.2})_3$ $(Sc_{0.888},Zr_{0.024},Mg_{0.08},Cu_{0.008})$. A closer look at the solid solution reveals that most of the Sc and Zr is supersaturated after casting even in the presence of Mg, Si and Cu. We discuss the impact of these results on the design of a suitable heat treatment for 6xxx-series alloys with Sc.

KEYWORDS

6xxx, Al_3Sc, Atom probe tomography, Dispersoids, Precipitation, Solidification

INTRODUCTION

The most common strategy to strengthen aluminum (Al) alloys is by micro-alloying to form a fine distribution of precipitates (Gladman, 1999). Whilst precipitates enhance the strength, this is often done to the detriment of ductility and corrosion performance (Davis, 1999). The 6xxx-series Al alloys are heavily used in the automotive industry as they offer an appropriate balance of strength, ductility and corrosion resistance (W. S. Miller et al., 2000). The strength increment in these alloys comes from the formation of the β'–Mg_2Si and the quaternary Q' phase (Chakrabarti & Laughlin, 2004; Polmear, St. John, Nie, & Qian, 2017). One opportunity to achieve stronger 6xxx-series alloys, whilst keeping good balance of corrosion resistance and formability, is the use of small additions of scandium (Sc).

Sc is one of the most potent strengtheners in Al alloys (Dorin, Ramajayam, Vahid, & Langan, 2018; Røyset & Ryum, 2005). Most of the strengthening benefits from Sc come from the formation of fine Al_3Sc dispersoids. The following strengthening mechanisms apply to Sc: 1) Solid solution strengthening, 2) precipitation hardening, 3) inhibiting recrystallization, 4) assisting nucleation of other strengthening phases (Dorin, Ramajayam, Lamb, & Langan, 2017). As compared to other dispersoid phases, Al_3Sc dispersoids have good electrochemical compatibility with Al alloys and hence do not affect their corrosion resistance (Cavanaugh, Birbilis, Buchheit, & Bovard, 2007). The coarsening resistance of Al_3Sc is often improved by adding zirconium (Zr), as it forms a Zr rich shell around Al_3Sc which prevents Sc from moving across the interface.

Research on the interactions between Mg, Si, Cu, Sc and Zr is very limited. However, it is the first step towards the development of Sc containing 6xxx-series alloys. Early research reported that Si content should be kept below 0.15wt% to draw the full benefits from Sc addition which would restrict its use in Al-Mg-Si alloys (Elagin, Zakharov, & Rostova, 1992). Indeed, impurity levels of Si (below 0.2wt%) were confirmed to enhance the precipitation kinetics of Al_3Sc (Beeri, Dunand, & Seidman, 2010; Booth-Morrison et al., 2012a; Du, Deng, Wang, Yan, & Rong, 2009; Vo, Dunand, & Seidman, 2014, 2016). Higher levels of Si were reported to be detrimental to the mechanical properties (Røyset, Hovland, & Ryum, 2002). The few studies looking at Sc and Zr in 6xxx-series alloys reported a refinement of the as-cast structure (Dang, Huang, & Cheng, 2009; Rokhlin, Bochvar, & Tarytina, 2015; Xiao, Song, & Wang, 2011). A recent study by Rokhlin et al. (Rokhlin et al., 2015) reports significant increase in strength in Sc and Zr containing 6xxx series alloys with medium Si level (0.2–0.36 wt.%). The conflicting results around the strengthening ability of Sc in Si containing alloys (6xxx series) in the separate studies may be related to the different solidification, cooling and heat treatment paths chosen.

The industrial application of Sc has been limited due to the high price of Sc and unreliable supply. A number of new initiatives underway will ease the Sc supply issues. As a result of this unreliable supply, previous works have explored the potential of utilizing elements that would substitute for Sc in Al_3Sc, such as Zr and Mg (Marquis, Seidman, Asta, & Woodward, 2006; Røyset & Ryum, 2005; Toropova, 1998). It is now also accepted that Si substitutes for Al in Al_3Sc (Booth-Morrison et al., 2012a, 2012b; De Luca, Dunand, & Seidman, 2016; Du et al., 2009; Erdeniz et al., 2017, Vo et al., 2014, 2016).

To the best of the authors' knowledge, there is no detailed research work looking at optimizing the path for precipitation of Sc-containing dispersoids and at understanding their subsequent impact on Mg-Si-Cu strengthening precipitates in Mg, Si, Cu, Sc, Zr containing alloys. A detailed understanding of this process is required to create a high strength Sc containing 6xxx-series with optimal distribution of fine Al_3Sc/Al_3Zr dispersoids and fine Mg-Si strengthening phases. When alloyed below their maximum solid solubility, Sc and Zr usually supersaturate during casting (Davydov, Rostova, Zakharov, Filatov, & Yelagin, 2000; Yin, Pan, Zhang, & Jiang, 2000). A two-step heat treatment is typically used to precipitate the Sc and Zr core-shell dispersoids from this solid solution (Deschamps, Lae, & Guyot, 2007). Recent work by Dorin et al. (2017) on an Al-4Cu-0.1Sc-0.2Zr (wt.%) alloy showed that stable dispersoids could be formed before extrusion, the Cu could be then solutionized and finally the fine θ'–Al_2Cu could be formed during a traditional ageing treatment. This optimized precipitate distribution was found to increase the yield strength by 150 MPa as compared to a reference Al-4Cu alloy. This work by Dorin et al. (2017)

challenged the initial idea that Cu had only a polluting effect on the Al_3Sc with the formation of the detrimental W–AlCuSc phase (Gazizov, Teleshov, Zakharov, & Kaibyshev, 2011; Lee, Wu, & Chen, 2015).

Optimizing the path for precipitation in Sc and Zr containing 6xxx-series alloys requires a detailed knowledge of the as-cast microstructure. The present work explores two model alloy compositions: an Al-Sc-Zr and an Al-Mg-Si-Cu-Sc-Zr. This microstructure is investigated using a combination of transmission electron microscopy and atom probe tomography. It is found that the presence of Mg and Si enhances the formation of dispersoids in the as-cast state. The composition of these dispersoids is quantitatively characterized and while it is found that Si substitutes to Al in the Al_3Sc structure, Mg, Zr and Cu are found to substitute to Sc. Mg and Cu are mainly found to partition at the α–Al/Al_3Sc interface. The impact of these different findings on the path to an optimal precipitate microstructure is further discussed.

MATERIALS AND EXPERIMENTAL METHOD

The model alloys used in this study were prepared using 99.999% pure Al and the following master alloys: Al-25wt.%Mg, Al-20wt.%Si, Al-33wt.%Cu, Al-2wt%Sc and Al-5wt%Zr. A small induction furnace was used for melting the alloys. The liquid metal was maintained at 710 ^{O}C for 30 minutes, under an argon atmosphere, before pouring into a cylindrical steel mold (80 mm in diameter x 200 mm tall). The cylindrical mold had a large steel base to provide directional solidification. The compositions of the alloys under study are detailed in Table 1. In order to compare the effect of the 6xxx-series alloying elements on the precipitate microstructure, Alloy 2 was alloyed with Sc, Zr, Mg, Si and Cu and Alloy 1 is the same alloy free from Mg, Si and Cu. Alloy 1 contained 0.05 wt.%Si which is lower than the traditional level of impurity in commercial Al alloys. The final cast ingots had a 4 kg weight.

Table 1. Compositions of the two alloys under study measured by ICP atomic emission spectroscopy. The nominal composition is specified in brackets.

Alloy		Al	Mg	Si	Sc	Zr	Cu
1	wt.%	Bal	-	0.03 (-)	0.09 (*0.1*)	0.13 (*0.2*)	-
	at.%	Bal	-	0.03 (-)	0.05	0.04	-
2	wt.%	Bal	1.01 (*1*)	0.60 (*0.6*)	0.09 (*0.1*)	0.19 (*0.2*)	0.2 (*0.2*)
	at.%	Bal	1.12	0.58	0.05	0.06	0.09

The equilibrium phase diagram of the studied alloys were generated using ThermoCalc ®™ with the latest TCAL5 database. The precipitates distribution was characterized in a JEOL 2100F transmission electron microscope (TEM) equipped with energy dispersive spectroscopy. TEM samples were prepared by electro-polishing in a solution of 33% nitric acid in methanol at -20 ^{O}C. Atom probe tomography (APT) was carried out on a LEAP 4000 HR instrument at a pulse fraction of 200 kHz, a temperature of 60 K, and pulse fraction of 20%. Samples were prepared by electro-polishing in a micro-loop apparatus under an optical microscope in a solution of 5% nitric acid in ethanol at room temperature (Gault, Moody, Cairney, & Ringer, 2012; M. K. Miller & Forbes, 2014). Electro-polished tips were given a final sharpen using Ga ions at 10 kV in a Quanta dual beam focused ion beam instrument.

RESULTS

Phase Diagrams

The phase diagrams of the two alloys under study were generated with ThermoCalc ®™ (Figure 1). The phase diagrams are plotted as a function of the Sc mass content. These diagrams give a good visual indication of the significant impact of adding Mg, Si and Cu on the thermodynamic of the alloy.

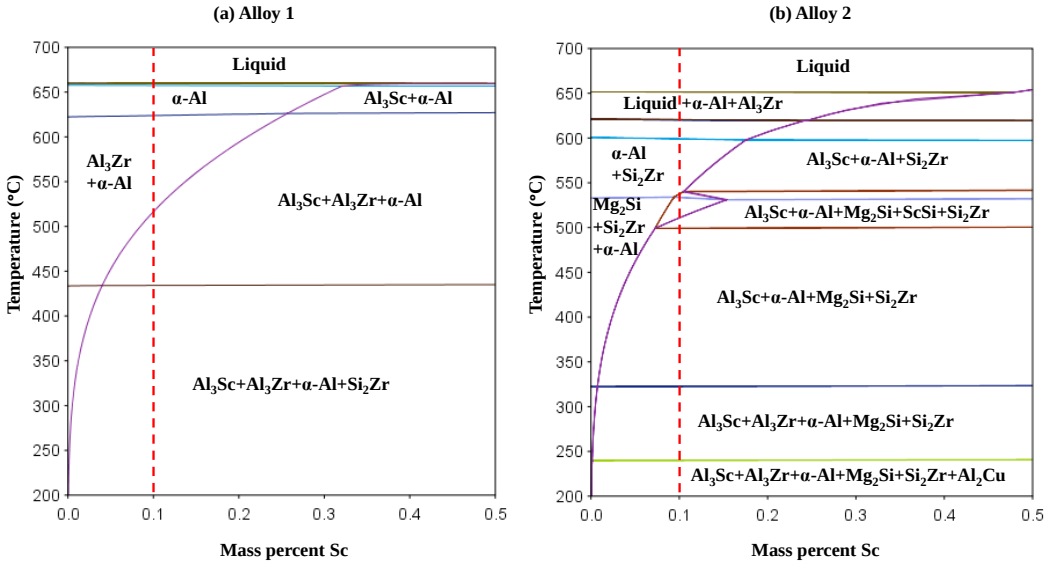

Figure 1. Phase diagrams as a function of Sc mass percent for (a) Al-0.05Si-0.1Sc-0.2Zr and (b) Al-1Mg-0.6Si-0.2Cu-0.1Sc-0.2Zr (in wt.%).

In alloy 1, a solid solution of α–Al can be obtained by heating above 623.8°C. As a result, solutionizing can be conducted in Al-Sc-Zr ternary alloys with low content of Sc and Zr (Fuller, Seidman, & Dunand, 2003). This is typically not required since the Sc and Zr are easily supersaturated during solidification and cooling (Davydov et al., 2000). The Al_3(Sc,Zr) dispersoids are then precipitated from the solid solution using a single or multiple step ageing treatment. Zr has a much lower diffusivity compared to Sc. Therefore, the Al_3(Sc,Zr) dispersoids are known to display inhomogeneous distribution of Sc and Zr atoms with the Zr atoms being concentrated on an outer rim around a Sc rich core (Forbord, Lefebvre, Danoix, Hallem, & Marthinsen, 2004). This core-shell morphology is usually preferred as it increases the coarsening resistance of the dispersoids. The use of a heat treatment in two steps can facilitate the formation of the core-shell morphology (Deschamps, Lae, & Guyot, 2007).

In alloy 2, the α–Al solid solution cannot be reached and the variety of phases is significantly increased. The ultimate goal, of optimal yield strength, is achieved by maximizing the fraction of Al_3Sc, Al_3Zr and Mg-Si strengthening precipitates and avoiding Si_2Zr and SiSc. The number density of the strengthening precipitates must also be maximized. The first step towards optimizing the precipitation path of the Sc containing 6xxx-series Al alloys lies in the understanding and quantification of the as-cast microstructure.

Transmission Electron Microscopy

Transmission electron microscopy was used to investigate the presence of precipitates in the as-cast microstructure, as shown in Figure 2. Alloy 1 was observed to be essentially free from precipitates, which confirms earlier results in the literature that low content of Sc and Zr supersaturate at traditional cooling rates (Davydov et al., 2000; Yin et al., 2000). Alloy 2, containing Mg, Si and Cu, exhibited a significantly different microstructure with the presence of a fine dispersion of precipitates with a size range 5–10 nm. These fine precipitates were observed to be homogeneously distributed within the sub-grains, as shown is the insert on Figure 2b. Coarser phases were observed to be present at sub-grain-boundaries. The absence of precipitates in Alloy 1 was confirmed by the absence of sub-lattice reflections in the selected area diffraction pattern. For Alloy 2, the position of the sub-reflections were typical of the $L1_2$ structure. Some higher order reflections were also observed and still need to be indexed.

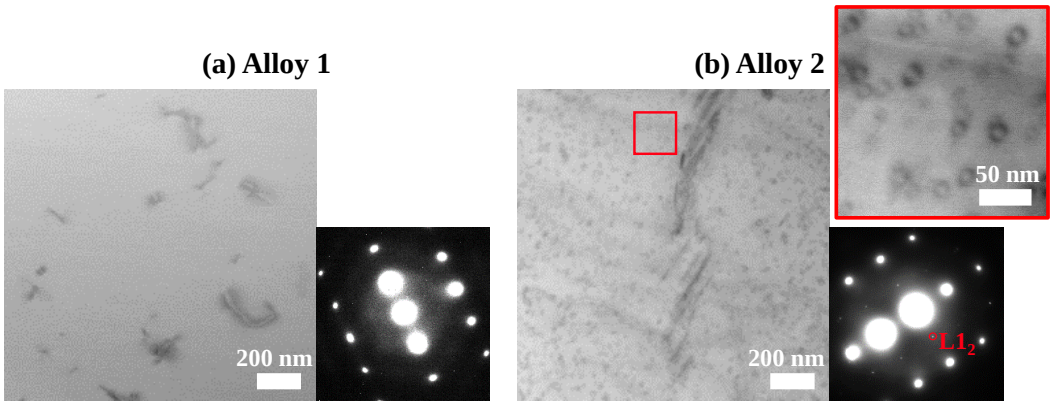

Figure 2. Bright field image in the <112> zone axis of (a) Alloy 1 and (b) Alloy 2.

Atom Probe Tomography (APT)

APT was conducted on alloy 2 in order to investigate the composition of the fine dispersoids observed in Figure 2b. Two volumes were collected from the as-cast condition, as shown in Figure 3. The compositions of the APT volumes were computed and compared with the bulk composition, as shown in Table 2. One can observe that there is good agreement between the two APT samples, suggesting a homogeneous distribution of the solute elements within the cast. The Sc and Zr contents in the APT samples correlated well with the bulk composition. This suggests there is only a small amount of Sc and Zr lost to coarse particles, such as intermetallics, and that they are mainly located within the as-cast dispersoids or supersaturated in the Al matrix. The contents in Mg, Si and Cu are lower than the bulk composition, which can be explained by the presence of coarse Mg-Si particles at the sub-grain boundaries, shown in Figure 2b. The presence of a few fine dispersoids was observed. At first sight, the observed particles seem to mainly contain Sc and Si which is consistent with earlier work that observed the substitution of Si into the Al_3Sc structure (Du et al., 2009).

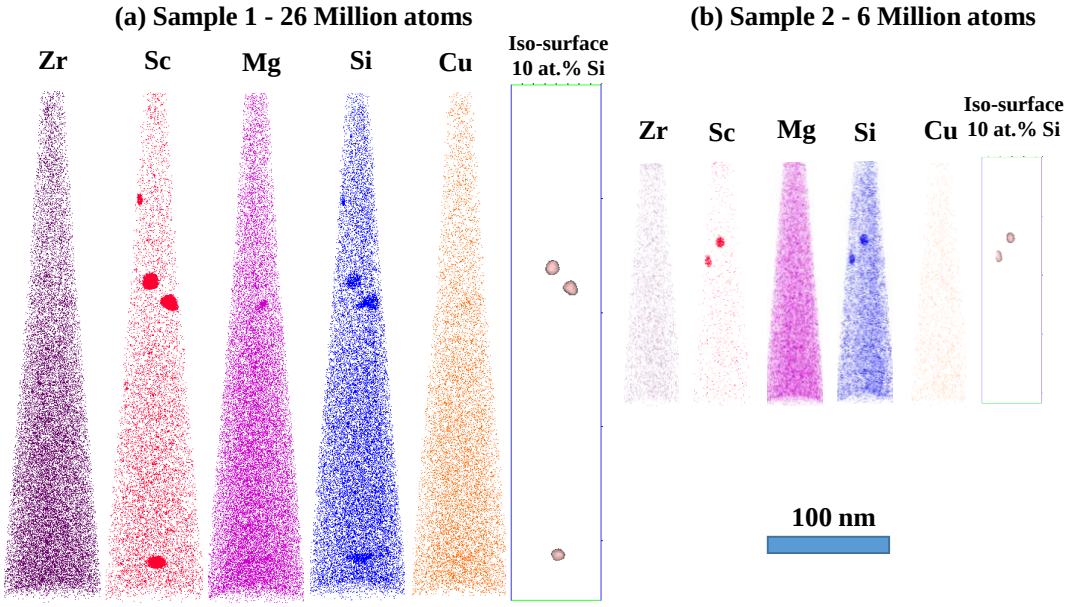

Figure 3. APT volumes of as-cast alloy 2. (a) Sample 1 – 26 M atoms and (b) Sample 2 – 6 M atoms.

Table 2. Composition of the two APT volumes and bulk composition in at.%.

Composition (at.%)	Al	Si	Sc	Zr	Mg	Cu
Sample 1	Bal	0.44	0.066	0.0510	0.66	0.032
Sample 2	Bal	0.37	0.046	0.044	0.7	0.034
Bulk	Bal	0.58	0.06	0.059	1.112	0.085

In order to further investigate the observed particles, an iso-concentration surface approach was used to define an interface between the particles and the α–Al solid solution. The strong partitioning of Mg at the dispersoid/Matrix interface was used to justify the use of an iso-concentration surface of 10 at.% Si. The segregation of Mg at the α–Al/Al_3Sc interface has already been reported elsewhere (Marquis et al., 2006). The proxygrams related to these iso-surfaces are displayed in Figure 4 for Sample 1 and Figure 5 for Sample 2. In these figures, the full proxygrams are represented on the left of the figure and a zoom is provided on the right to look at the minor elements in the Al_3Sc structure. These proxygrams reveal that the particles are rich in Al, Sc and Si and that Mg partitions at the dispersoids' interface. Zr is found to be present within the particles and there is no sign of core-shell morphology. A slight Cu partitioning is also observed at the α–Al/Al_3Sc interface.

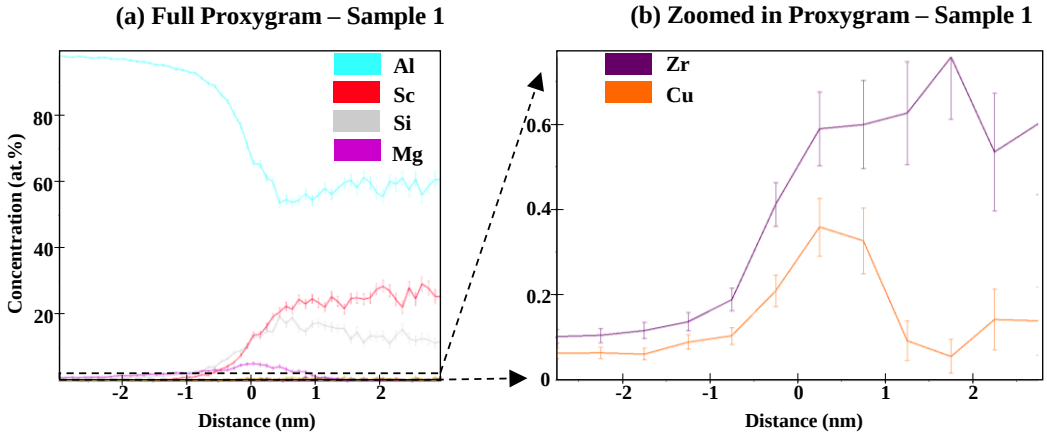

Figure 4. (a) Proxygram from sample 1 using 10 at.% Si iso-surfaces and (b) zoomed in proxygram.

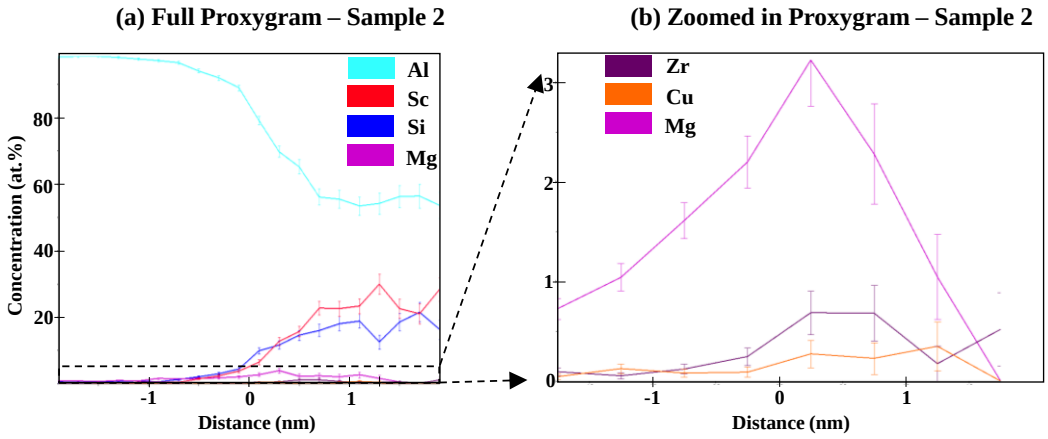

Figure 5. (a) Proxygram from sample 2 using 10 at.% Si iso-surfaces and (b) zoomed in proxygram.

The composition of the five dispersoids observed (composition within the iso-surfaces) are reported in Table 3. The average dispersoid composition is computed and the standard deviation calculated. The standard deviation for the content of the three major elements (Al, Si and Sc) is relatively low; within 10% of the average value. The error is larger for the content of minor elements (Mg, Zr and Cu) within the dispersoids.

Table 3. Compositions of the five dispersoids observed in Sample 1 and Sample 2 (Figure 3). The average dispersoid composition and related standard deviations are computed.

Dispersoids (at.%)	Al	Si	Sc	Zr	Mg	Cu
1	59.4	14.3	22.3	0.61	2.18	0.24
2	60.0	14.9	22.2	0.48	1.47	0.12
3	57.7	14.9	24.0	0.58	2.20	0.22
4	59.6	15.5	21.1	0.56	1.80	0.11
5	62.6	14.5	18.4	0.64	2.20	0.27
Average	59.9	14.8	21.6	0.57	1.97	0.19
Std Dev	1.58	0.41	1.85	0.05	0.29	0.06

APT is the most powerful tool to quantify the solid solution (De Geuser & Lefebvre, 2011). The study of the solid solution is an indirect way of quantifying the precipitation state within the bulk microstructure. The composition of the solid solution (outside of the iso-concentration surfaces) for both samples is reported in Table 4. The average solid solution is calculated and compared to the bulk alloy composition (Table 4). Finally, the percentage of solute retained in solid solution is computed (Table 4). These results show that a significant amount of Sc and Zr is still retained in solid solution in the as-cast microstructure. Mg, Si and Cu are still in solid solution in significant levels, although a non-negligible amount has been consumed by the formation of larger particles, most likely similar to the sub-grain boundary particles observed in Figure 2b.

Table 4. Compositions of the solid solution measured in Sample 1 and Sample 2 (Figure 3). The average solid solution is compared with the bulk composition. The percentage of solute retained in the solid solution is calculated.

Solid solution (at.%)	Al	Si	Sc	Zr	Mg	Cu
Sample 1	98.5	0.44	0.059	0.051	0.66	0.032
Sample 2	98.5	0.36	0.043	0.045	0.70	0.034
Average SS	98.5	0.40	0.051	0.048	0.68	0.035
Bulk	Bal	0.58	0.060	0.059	1.11	0.085
% in solid sol	/	69%	85%	81%	61%	41%

DISCUSSION

Alloys 1 and 2 were cast, solidified and cooled under the same conditions. Results from TEM show that the Sc and Zr remain in solution for the ternary Al-Sc-Zr alloy 1 (Figure 2a). This result confirms the results by (Davydov et al., 2000) who report that Sc and Zr supersaturate during continuous casting of ingots up to 800 mm in diameter. Fine Sc-containing dispersoids were observed in the as cast condition for Alloy 2 (Figure 2b). Despite the formation of these Sc containing dispersoids, 85% of the Sc and 81% of the Zr remained in solution after casting (Table 4). Such a supersaturation level indicates that a large part of Sc and Zr is still available as solute for the formation of fine dispersoids during a controlled homogenization treatment. The difficulty lies in finding the right heat treatment path that leads to an ideal distribution of dispersoids.

As-Solidified Dispersoids

The dispersoids observed in alloy 2 have a $L1_2$ crystal structure, as confirmed in the selected area diffraction patterns, and a M_3X type stoichiometry. In order to respect this stoichiometry, the Si is found to substitute to Al and Zr, Mg and Cu substitute to Sc. The resulting average dispersoid composition is: $(Al_{0.8},Si_{0.2})_3$ $(Sc_{0.888},Zr_{0.024},Mg_{0.08},Cu_{0.008})$. The substitution of Al by 20 at.%Si is the largest reported in the literature where the usual substitution is below 10 at.% even at the onset of precipitation. This high Si content within Al_3Sc can be due to either or both of two things: 1) the Si content within the alloy is larger than the Si content investigated in the literature, 2) the dispersoids observed herein are formed upon cooling rather than during an isothermal treatment.

Substitution of Si for Al in Al_3Sc

Si is always present in commercial Al alloys at impurity levels (up to 0.2 wt.%). Therefore, it is important to understand the impact of Si on the formation of Al_3Sc. Previous studies have looked at the effect of low Si content, i.e. 0.02 at.% versus 0.06 at.% (Booth-Morrison et al., 2012a). A significant effect of Si on the precipitation kinetics of Al_3Sc was reported when compared to an alloy virtually free from Si. The increase in kinetics was explained by attractive Si-Sc binding energies at the first and second nearest-neighbor distances which leads to a strong tendency for Si and Sc to cluster. From these earlier studies, it is clear that the Si-Sc clustering is one of the main driving forces for the nucleation of Al_3Sc in all Sc-containing Al alloys. The effect of Al_3Sc nucleation in alloys with higher Si content, such as 6xxx series, has not yet been studied. The Si-to-Al ratio in Al_3Sc has been computed from separate studies and displayed in Figure 6 (Booth-Morrison et al., 2012a, 2012b; De Luca et al., 2016; Du et al., 2009; Erdeniz et al., 2017, Vo et al., 2014, 2016). These previous studies investigated the composition of dispersoids in different ageing conditions. Based on the diffusion coefficient of Si in Al (Mantina, Wang, Chen, Liu, & Wolverton, 2009), an equivalent time at 300°C is calculated, which allows grouping of all the data on a single graph. The initial Si content within the alloy seems to have little impact on the Si content within the dispersoids and the Si to Al ratio is found to plateau around 0.02. For alloy 2 and assuming stoichiometry is respected, the volume fraction of Al_3Sc at equilibrium would be approximately 0.24%. At an Al to Si ratio of 0.02 in Al_3Sc, this would mean that ~0.015 at.%Si would go to Al_3Sc, still leaving most of the 0.58 at.%Si available to form Mg_2Si precipitates. As a result, the main impact of a high Si content is to activate nucleation of the dispersoids as early as during solidification.

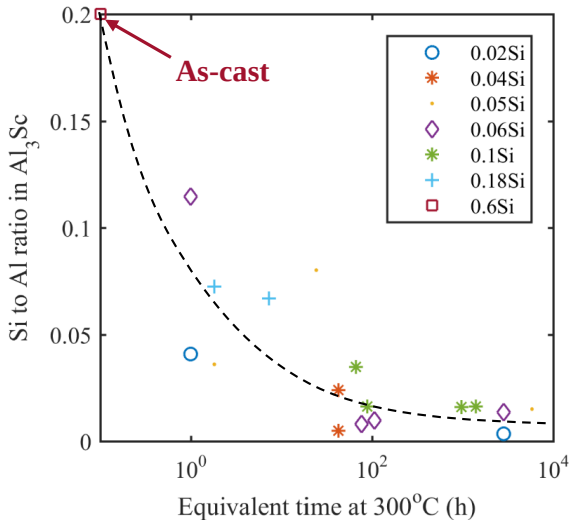

Figure 6. Si to Al ratio in Al_3Sc as a function of an equivalent ageing time at 300 °C for different Si content in the studied alloy. Data from (Booth-Morrison et al., 2012a, 2012b; De Luca et al., 2016; Du et al., 2009; Erdeniz et al., 2017, Vo et al., 2014, 2016).

Segregation at the α–Al/Al_3Sc Interface

The tendency for Mg to partition at the coherent α–Al/Al_3Sc interfaces was earlier demonstrated by first-principle (Asta, Ozolins, & Woodward, 2001) and ab-initio (Marquis et al., 2006) calculations. Previous work by (Marquis et al., 2006) showed that the level of Mg segregation was constant as a function of ageing time. In the samples studied here, the Mg concentration is found to peak at ~5 at.% and ~3 at.% respectively for Samples 1 and 2, which is comparable to the values reported by (Marquis et al., 2006). This segregation will potentially assist the nucleation of the strengthening precipitates on the dispersoids, as was recently shown in an Al-Cu-Sc-Zr alloy (Dorin et al., 2017).

Consequence for Heat Treatment Design in a Sc Containing 6xxx-series Alloy

The solid solution analysis reveals that most of the Sc and Zr is still available as solute in the as cast condition. As a result, an initial solution treatment to re-dissolve the as-cast dispersoids may not be required. An aging schedule that brings the Sc and Zr out of solution without over coarsening the dispersoids present after casting could be used in this approach. If this cannot be accomplished it may be necessary to dissolve these dispersoids first and then use a multiple-step aging approach to form Al_3Sc-core/Al_3Zr-shell dispersoids. The goal of these aging treatments is to form Sc-containing dispersoids that can survive the extrusion/rolling/forging steps required for production of commercial Al-Mg-Si 6xxx alloys.

CONCLUSIONS

In the present study, the impact of adding Mg, Si and Cu on the solidification behavior of Al-Sc-Zr was investigated. A model alloy approach was used and the main conclusions are as follows:

- An Si-assisted mechanism allows nucleation of Al_3Sc dispersoids during solidification.
- The composition of the as-solidified dispersoids is $(Al_{0.8},Si_{0.2})_3$ $(Sc_{0.888},Zr_{0.024},Mg_{0.08},Cu_{0.008})$.
- Most of the Sc and Zr is found to supersaturate despite the presence of Si. This suggests that it may be possible to develop aging treatments that will precipitate Sc / Zr dispersoids from the as-cast condition with no need for prior solution treatment.
- The as-solidified dispersoids do not display a core-shell morphology. Mg and Cu are found to partition at the α–Al/Al_3Sc interface.

REFERENCES

Asta, M., Ozolins, V., & Woodward, C. (2001). A first-principles approach to modeling alloy phase equilibria. *OM Journal of the Minerals, Metals and Materials Society*, *53*(9), 16–19.

Beeri, O., Dunand, D. C., & Seidman, D. N. (2010). Roles of impurities on precipitation kinetics of dilute Al–Sc alloys. Materials Science and Engineering: A, 527(15), 3501–3509.

Booth-Morrison, C., Mao, Z., Diaz, M., Dunand, D C., Wolverton, C., & Seidman, D. N. (2012a). Role of silicon in accelerating the nucleation of Al3(Sc,Zr) precipitates in dilute Al–Sc–Zr alloys. Acta Materialia, 60(12), 4740–4752.

Booth-Morrison, C., Seidman, D. N., & Dunand, D. C. (2012b). Effect of Er additions on ambient and high-temperature strength of precipitation-strengthened Al–Zr–Sc–Si alloys. Acta Materialia, 60(8), 3643–3654.

Cavanaugh, M. K., Birbilis, N., Buchheit, R. G., & Bovard, F. (2007). Investigating localized corrosion susceptibility arising from Sc containing intermetallic Al3Sc in high strength Al-alloys. Scripta Materialia, 56(11), 995–998.

Chakrabarti, D. J., & Laughlin, D. E. (2004). Phase relations and precipitation in Al–Mg–Si alloys with Cu additions. Progress in Materials Science, 49(3), 389–410.

Dang, J., Huang, Y., & Cheng, J. (2009). Effect of Sc and Zr on microstructures and mechanical properties of as-cast Al-Mg-Si-Mn alloys. Trans. of Nonferrous Met. Soc. of China, 19(3), 540–544.

Davis, J. R. (1999). Corrosion of aluminum and aluminum alloys. Asm International.

Davydov, V. G., Rostova, T. D., Zakharov, V. V., Filatov, Y. A., & Yelagin, V. I. (2000). Scientific principles of making an alloying addition of sc to aluminium alloys. Mat. Sci. Eng.: A, 280(1), 30–36.

De Geuser, F., & Lefebvre, W. (2011). Determination of matrix composition based on solute-solute nearest-neighbor distances in atom probe tomography. Micro. Res. and Technique, 74(3), 257–263.

De Luca, A., Dunand, D. C., & Seidman, D. N. (2016). Mechanical properties and optimization of the aging of a dilute Al-Sc-Er-Zr-Si alloy with a high Zr/Sc ratio. Acta Materialia, 119, 35–42.

Deschamps, A., Lae, L., & Guyot, P. (2007). In situ small-angle scattering study of the precipitation kinetics in an Al–Zr–Sc alloy. Acta Materialia, 55(8), 2775–2783.

Dorin, T., Ramajayam, M., Lamb, J., & Langan, T. J. (2017). Effect of Sc and Zr additions on the microstructure/strength of Al-Cu binary alloys. Materials Science and Engineering A.

Dorin, T., Ramajayam, M., Vahid, A., & Langan, T. J. (2018). Chapter 17: Aluminium Scandium Alloys. In Fundamentals of Aluminium Metallurgy: Recent Advances. Elsevier.

Du, G., Deng, J., Wang, Y., Yan, D., & Rong, L. (2009). Precipitation of (Al,Si)3Sc in an Al-Sc-Si alloy. Scripta Materialia, 61(5), 532–535.

Elagin, V. I., Zakharov, V. V., & Rostova, T. D. (1992). Scandium-alloyed aluminum alloys. Metal Science and Heat Treatment, 34(1), 37–45.

Erdeniz, D., Nasim, W., Malik, J., Yost, A. R., Park, S., De Luca, A., Dunand, D. C. (2017). Effect of vanadium micro-alloying on the microstructural evolution and creep behavior of Al-Er-Sc-Zr-Si alloys. Acta Materialia, 124, 501–512.

Forbord, B., Lefebvre, W., Danoix, F., Hallem, H., & Marthinsen, K. (2004). Three dimensional atom probe investigation on the formation of Al3(Sc, Zr) in al alloys. Scripta Materialia, 51(4), 333–337.

Fuller, C. B., Seidman, D. N., & Dunand, D. C. (2003). Mechanical properties of Al (Sc, Zr) alloys at ambient and elevated temperatures. Acta Materialia, 51(16), 4803–4814.

Gault, B., Moody, M. P., Cairney, J. M., & Ringer, S. P. (2012). Atom probe microscopy (Vol. 160). Springer Science & Business Media.

Gazizov, M., Teleshov, V., Zakharov, V., & Kaibyshev, R. (2011). Solidification behaviour and the effects of homogenisation on the structure of an Al-Cu-Mg-Ag-Sc alloy. Journal of Alloys and Compounds, 509(39), 9497–9507.

Gladman, T. (1999). Precipitation hardening in metals. Mat. Sci. and Tech., 15(1), 30–36.

Lee, S.-L., Wu, C.-T., & Chen, Y.-D. (2015). Effects of Minor Sc and Zr on the Microstructure and Mechanical Properties of Al-4.6Cu-0.3Mg-0.6Ag Alloys. J. Mat. Eng. and Perf., 24(3), 1165–1172.

Mantina, M., Wang, Y., Chen, L. Q., Liu, Z. K., & Wolverton, C. (2009). First principles impurity diffusion coefficients. Acta Materialia, 57(14), 4102–4108.

Marquis, E. A., Seidman, D. N., Asta, M., & Woodward, C. (2006). Composition evolution of nanoscale Al3Sc precipitates in an Al–Mg–Sc alloy: Experiments and computations. Acta Materialia, 54(1), 119–130.

Miller, M. K., & Forbes, R. G. (2014). Atom-probe tomography: the local electrode atom probe.

Miller, W. S., Zhuang, L., Bottema, J., Wittebrood, A. J., De Smet, P., Haszler, A., & Vieregge, A. (2000). Recent development in al alloys for the automotive industry. Mat. Sci. Eng.: A, 280(1), 37–49.

Polmear, I., St. John, D., Nie, J.-F., & Qian, M. (2017). Light alloys: metallurgy of the light metals. Butterworth-Heinemann.

Rokhlin, L. L., Bochvar, N. R., & Tarytina, I. E. (2015). Joint effect of scandium and zirconium on the structure and the strength properties of Al–Mg2Si–Based alloys. Russ. Met., 2015(9), 726–731.

Røyset, J., Hovland, H., Ryum, N. (2002). An investigation of dilute Al-Sc-Si alloys (Vol. 396–402).

Røyset, J., & Ryum, N. (2005). Scandium in aluminium alloys. Int. Mat. Rev., 50(1), 19–44.

Toropova, L. S. (1998). Advanced aluminum alloys containing scandium: structure and properties. Taylor & Francis.

Vo, N. Q., Dunand, D. C., & Seidman, D. N. (2014). Improving aging and creep resistance in a dilute Al–Sc alloy by microalloying with Si, Zr and Er. Acta Materialia, 63, 73–85.

Vo, N. Q., Dunand, D. C., & Seidman, D. N. (2016). Role of silicon in the precipitation kinetics of dilute Al-Sc-Er-Zr alloys. Materials Science and Engineering A, 677, 485–495.

Xiao, D., Song, M., & Wang, S. (2011). Effects of minor Sc and heat treatment on microstructure and mechanical properties of AA6022 alloy. Tezhong Zhuzao Ji Youse Hejin/Special Casting and Nonferrous Alloys, 31(1), 8–11.

Yin, Z., Pan, Q., Zhang, Y., & Jiang, F. (2000). Effect of minor Sc and Zr on the microstructure and mechanical properties of Al–Mg based alloys. Materials Science and Engineering: A, 280(1), 151–155.